Measurement of ^{232}Th(n,γ) reaction cross sections in the neutron energy range of 11–19 MeV

Siddharth Parashari,[1,*] S. Mukherjee,[1,†] A. P. Singh,[2] Vibha Vansola,[1] H. Naik,[3] B. K. Nayak,[4] Rajnikant Makwana,[1] S. V. Suryanarayana,[4] N. L. Singh,[1] Mayur Mehta,[5] Y. S. Sheela,[6] M. Karkera,[6] R. D. Chauhan,[1] and S. C. Sharma[4]

[1]*Department of Physics, Faculty of Science, The Maharaja Sayajirao University of Baroda, Vadodara 390002, India*
[2]*Department of Statistics, Banaras Hindu University, Varanasi 221005, India*
[3]*Radiochemistry Division, Bhabha Atomic Research Center, Mumbai 400085, India*
[4]*Nuclear Physics Division, Bhabha Atomic Research Center, Mumbai 400085, India*
[5]*Institute for Plasma Research, Gandhinagar, Gujarat 382428, India*
[6]*Department of Statistics, Manipal University, Manipal 576104, India*

(Received 24 August 2017; revised manuscript received 15 June 2018; published 30 July 2018)

The cross sections for the ^{232}Th(n,γ) reaction have been measured in the neutron energy range of 11–19 MeV by using activation and offline γ-ray spectrometric techniques. The neutrons of desired energy were obtained by the ^{7}Li(p,n) reaction using a proton beam of 13–21 MeV from the 14UD BARC-TIFR Pelletron facility at Mumbai, India. The ^{232}Th(n,γ) reaction cross sections were calculated using the computer code TALYS-1.8. The uncertainties in the measurement have been studied using covariance analysis of the experimental data. The results from the present work have been compared with the evaluated data of ENDF/B-VII.1 and JENDL-4.0 as well as the theoretically calculated values based on TALYS-1.8, and were found to be in good agreement. The outcome of the present work is important for the development of future fast reactors and accelerator driven subcritical systems (ADSs).

DOI: 10.1103/PhysRevC.98.014625

I. INTRODUCTION

The nuclear technology used for power production has no greenhouse gas emission effect. Thus nuclear power has a potential to expand in large scale and can effectively replace fossil fuel. However, nuclear power production in conventional reactors based on enriched or natural uranium fuel has a problem of generation of long-lived minor actinides. The issues of global warming and long-lived nuclear waste management can be avoided by using a nuclear power reactor based on thorium-uranium fuel. Owing to a number of favorable material characteristics, ^{232}Th is a better fertile host [1] to produce the fissile ^{233}U isotope. Rubbia *et al.* [2] and Bowman [3,4] have proposed the concept of accelerator-driven subcritical reactor systems (ADSs), which demonstrate that a commercial nuclear power plant of adequate power can also be built around a subcritical reactor, provided it can be fed externally with the required intensity of accelerator-produced neutrons. ADSs have attractive features [5–8] for the elimination of troublesome long-lived minor actinides (^{237}Np, ^{240}Pu, ^{241}Am, ^{243}Am, ^{244}Cm) and fission products (^{93}Zr, ^{99}Tc, ^{109}Pd, ^{129}I, ^{135}Cs) of the spent fuel, as well as for nuclear energy generation utilizing thorium as fuel. Besides ADSs, advanced heavy water reactors (AHWRs) [9,10] and fast reactors [11–13] are also of current interest for power production. In the Th-U fuel cycle, the production of the fissile nucleus ^{233}U depends on the ^{232}Th(n,γ) reaction cross sectionwhich is required with an accuracy of 1–2% for predicting the dynamical behavior of complex arrangements in fast reactors and ADSs [14,15] safely. In fast breeder reactors, the most important region for neutron capture of ^{232}Th lies between 10 and 100 keV [16], but ADSs will use fast neutrons. Thus the ^{232}Th(n,γ) reaction cross section at higher neutron energy has a strong impact on the performance and safety assessment for ADSs [17]. In ADSs a 10% change in the ^{232}Th neutron capture cross section gives rise to a 30% change in the needed proton current of the accelerator if the system has to be operated at a subcritical level of $K_{\text{eff}} \approx 0.97$ [18].

The cross-section data for the ^{232}Th(n,γ) reaction are available in the literature over a wide range of neutron energies from thermal to 2.73 MeV, based on physical measurements [19–21] and activation technique [22–32]. Beyond 2.73 MeV, the data for the ^{232}Th(n,γ) reaction cross section are available at the neutron energy of 3.7 MeV [24,26] and around 6–17 MeV [25,28–30,33] by using the activation technique. However, the data at the neutron energy of 14.5 MeV [33] are significantly higher than the expected trend by others [25,28–30]. From these data, it can be observed that the ^{232}Th(n,γ) reaction cross section decreases monotonically from 20 eV to 2.73 MeV. However, sufficient data are not available in the literature except for a few [24,25,28–30,33] above the neutron energy of 2.73 MeV. In view of this, in the present work, we have measured the ^{232}Th(n,γ) reaction cross section at average neutron energies of 10.95 ± 0.59, 13.97 ± 0.57, 14.98 ± 0.55, and 18.99 ± 0.65 MeV by using the activation and offline γ-ray spectrometric techniques. The neutron beam was generated by using the ^{7}Li(p,n) reaction with proton energies of 13, 16, 17, and 21 MeV. A detailed covariance analysis has

*siddharthparashri5@gmail.com
†sk.mukherjee-phy@msubaroda.ac.in

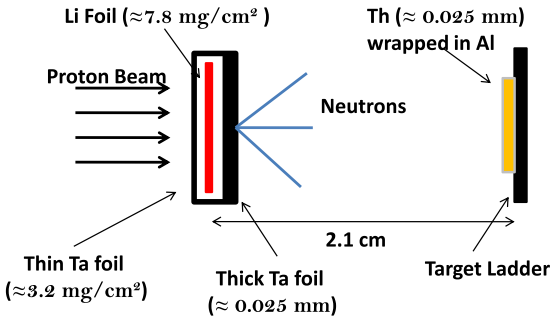

FIG. 1. Experimental setup used for the irradiations.

also been performed to understand the dependence of cross section on uncertainties from different parameters. The present data are of particular interest from the point of view of the giant dipole resonance (GDR) around the neutron energies of 10–20 MeV.

This paper is divided into the following sections: the experimental methodology is given in Sec. II. Section III gives the data analysis. Covariance analysis of the experimental uncertainty is described in Sec. IV. Section V gives the results and discussion, followed by conclusions in Sec. VI.

II. EXPERIMENTAL METHODOLOGY

The experiment was carried out by using the 14UD Bhabha Atomic Research Center–Tata Institute of Fundamental Research (BARC-TIFR) Pelletron facility in Mumbai, India, using the activation technique followed by offline γ-ray spectroscopy. Proton beams of known energy from the pelletron were bombard on a lithium (Li) target to generate the desired energy neutron beam from the $^{7}\mathrm{Li}(p,n)$ reaction. A Li foil of thickness ≈ 7.8 mg/cm^2 was sandwiched between tantalum (Ta) foils of different thicknesses. Thin Ta foil ≈ 3.2 mg/cm^2 was used at the beam side to ensure that protons passing through the foil should not lose much energy, while a thick Ta foil more than 0.025 mm thick was used at the back of the Li foil to stop the proton beam. Behind the Ta-Li-Ta stack, a ^{232}Th sample of thickness ≈ 0.025 mm was placed at a distance of 2.1 cm, aligned at zero degrees with respect to the proton beam. The ^{232}Th sample was wrapped with pure aluminum foil of thickness 0.025 mm to prevent the contamination of radioactivity coming out od the sample to the surroundings during irradiation. The experimental arrangement of the stack used for the irradiation is shown in Fig. 1. The stack was kept inside the irradiation port at 6 m height just before analyzing magnets on the main beamline of the Pelletron. This port is very suitable for such kind of irradiation as it provides high proton flux. The energy spread for protons at 6 m height of the beamline was 50–90 keV. At this port, the terminal voltage was regulated by a generating voltmeter (GVM) using a terminal potential stabilizer. Further, a collimator of 6 mm diameter was used as the target in order to get a proper circular shaped beam.

The irradiation for each sample was carried out for about 5–8 h so that sufficient activity could be built up to be suitable for the γ-ray counting. The proton energies used in the irradiations were 13, 16, 17, and 21 MeV. The degradation of proton energy in the Li and Ta metal foils facing the beam was calculated using the computer code SRIM [34]. The neutrons thus generated by the $^{7}\mathrm{Li}(p,n)$ reaction were found to have average energies of 10.95 ± 0.59, 13.97 ± 0.57, 14.98 ± 0.55, and 18.99 ± 0.65 MeV, respectively. After the irradiation, each sample was counted for a sufficiently long time due to the half-life of 26.97 days for ^{233}Pa, which is the daughter product of ^{233}Th. The γ-ray counting of the samples was done by using a precalibrated 80 cm^3 HPGe detector coupled to a PC based 4096 channel analyzer. A standard ^{152}Eu source was used for the energy and efficiency calibration. The resolution of the detector system during counting was measured as 2.0 keV at 1332 keV of ^{60}Co. The samples were placed at a suitable distance from the endcap of the detector to avoid summing error. The irradiated Th samples were counted for a sufficient amount of time to accumulate sufficient data and also to minimize the counting statistic uncertainty.

III. DATA ANALYSIS

A. Calculations for neutron spectra

The incident proton energies used in the present experiment for irradiation purposes were 13, 16, 17, and 21 MeV. Neutrons were generated by the $^{7}\mathrm{Li}(p,n)$ reaction using the protons as the incident particle on a natural Li target wrapped with Ta foil. Natural lithium consists of ^{6}Li and ^{7}Li isotopes with abundances of 7.42% and 92.58%, respectively. Therefore, a variety of reactions takes place when the protons interact with the natural lithium target. The production of the ground state of ^{7}Be from the $^{7}\mathrm{Li}(p,n)$ reaction has a threshold energy of 1.88 MeV, whereas the threshold energy for the first excited state is 2.38 MeV. Thus above the proton energy of 2.38 MeV ($E_P \geqslant 2.4$ MeV) a second neutron group is produced due to the population of the first excited state of ^{7}Be. Thus, for the proton energies of 13, 16, 17, and 21 MeV, neutron energies corresponding to the ground state of ^{7}Be are 11.12, 14.12, 15.12, and 19.12 MeV, which are referred to as the first group (n_0). For the first excited state of ^{7}Be, the neutron energies of the second group of neutrons (n_1) will be 10.62, 13.62, 14.62, and 16.62 MeV, respectively. Besides n_0 and n_1 groups of neutrons, other reaction channels such as $^{7}\mathrm{Li}(p,\gamma)^{8}\mathrm{Be} \rightarrow {}^{4}\mathrm{He} + {}^{3}\mathrm{He} + n$ ($Q = -3.23$ MeV) also open up at such high proton energies, which results in a continuous neutron energy distribution. In the present work, the continuous neutron spectrum was generated by using the neutron energy distribution given in Refs. [35,36]. The resulting neutron fluxes (ϕ_i) for proton energies of 16 and 21 MeV are shown in Fig. 2. These distributions were obtained by shifting the peak wherever necessary, and interpolation was also used to shift the peak for desired neutron energies. This scaling was done because the maximum neutron energy from the $^{7}\mathrm{Li}(p,n)$ reaction cannot exceed $E_P - 1.88$ MeV. Similarly, for $E_P = 13$ and 17 MeV, the corresponding neutron spectra are obtained by interpolation of the neutron distributions of Mashnik *et al.* [36]. These neutron spectra have a quasi-monoenergetic the peak near $E_P - 1.88$ MeV and a long tail towards the lower energies, as shown in Fig. 2. The tail

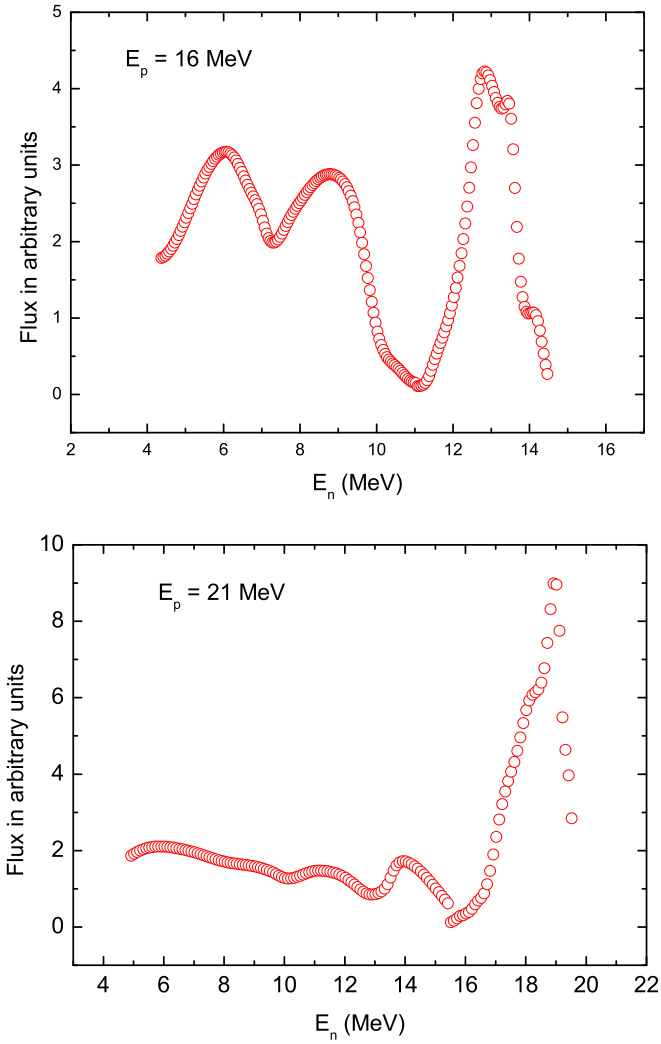

FIG. 2. Neutron spectra generated from the ^{7}Li(p,n) reaction using 16 and 21 MeV protons.

region consisting of lower neutron energies also contributes in the reaction cross sections. Therefore, it is necessary to remove the contribution arising from the tail part of the neutron spectra. This correction can be done by considering spectral average cross sections as given in the next section.

B. Calculation of neutron flux

The generated neutron spectra were used for the calculation of the total neutron flux, which was produced by the ^{7}Li(p,n) reaction. In the present experiment, we have used the Th sample itself as the neutron flux monitor by using the yields of fission products such as ^{97}Zr ($t_{1/2} = 16.9$ h, $E_\gamma = 743$ keV) [37]. We did the γ-ray counting for ^{97}Zr by considering its half-life. The total ^{232}Th(n,f) reaction cross sections for all the possible neutron energies in the spectra were taken from ENDF/B-VII.1 [38]. A spectra weighted cross section ($\langle\sigma_W\rangle$) for the ^{232}Th(n,f) reaction was calculated by using [39]

$$\langle\sigma_W\rangle = \frac{\sum_{E_i}\phi_{E_i}\sigma_{E_i}}{\sum_{E_i}\phi_{E_i}}, \tag{1}$$

where ϕ_{E_i} and σ_{E_i} are the neutron flux and corresponding cross section respectively, taken from ENDF/B-VII.1. Then the total neutron flux was calculated by using the following expression:

$$\langle\Phi\rangle = \frac{C_{\rm obs}\lambda\left(\frac{\rm CL}{\rm LT}\right)}{N_0 I_\gamma \epsilon \langle\sigma_W\rangle Y(1-e^{-\lambda t_i})(e^{-\lambda t_c})(1-e^{-\lambda LT})} \tag{2}$$

where, $C_{\rm obs}$ is the observed count for the respective γ ray, CL and LT are the clock time and the live time for the counting of the spectrum, λ is the decay constant ($\frac{0.693}{t_{1/2}}$), I_γ is the branching ratio for the respective γ ray taken from Ref. [37], N_0 is the total number of target nuclei in the sample, ϵ is the detector efficiency, and Y is the yield of ^{97}Zr (at 14 MeV neutron energy) taken from Refs. [40–42]. t_i and t_c are the irradiation time and cooling time respectively. The spectroscopic data related to flux calculations are given in Table I. The flux values thus extracted from the above-mentioned method were used in the calculation of the (n,γ) reaction cross section for ^{232}Th.

C. Determination of ^{232}Th(n,γ) reaction cross sections

The ^{232}Th(n,γ) reaction leads to the formation of ^{233}Th, which undergoes β decay to produce its daughter product ^{233}Pa. The decay scheme related to present reaction is shown below and the spectroscopic data used in the calculation are given in Table I:

$$^{232}\text{Th}(n,\gamma) \rightarrow {}^{233}\text{Th} \xrightarrow{\beta^-} {}^{233}\text{Pa} \xrightarrow{\beta^-} {}^{233}\text{U}$$
$$(1.405\times10^5\ \text{yr}) \quad (21.23\ \text{min}) \quad (26.97\ \text{d}) \quad (1.52\times10^5\ \text{yr})$$

TABLE I. Nuclear spectroscopic data of radionuclides taken from Ref. [37].

Reaction	Spin state J^π	$T_{1/2}$	Decay mode (%)	E_γ (KeV)	I_γ (%)
^{232}Th$(n,f)^{97}$Zr	$1/2^+$	16.749 ± 0.008 h	β^-(100)	743.36 ± 0.06	93.09 ± 0.01
^{232}Th$(n,\gamma)^{232}$Th	$1/2^+$	21.83 ± 0.04 min	β^-(100)		
^{233}Th $\longrightarrow \beta^-$ ^{233}Pa	$3/2^+$	26.975 ± 0.013 d	β^-(100)	311.90 ± 0.05	38.5 ± 0.4

TABLE II. ^{232}Th(n,γ) reaction cross-sections at different neutron energies (before and after tailing correction).

Neutron Energy (MeV)	Cross section (mb)			
	Measured	Tailing part		Final
		ENDF-B/VII.1	JENDL-4.0	
10.95 ± 0.59	14.45 ± 3.48	12.56	12.76	1.787
13.97 ± 0.57	2.79 ± 0.71	1.458	1.706	1.207
14.98 ± 0.55	3.37 ± 0.69	1.983	2.315	1.22
18.99 ± 0.65	1.16 ± 0.14	0.579	0.682	0.529

Since ^{233}Th ($t_{1/2} = 21.83$ min) undergoes β^- decay to produce ^{233}Pa ($t_{1/2} = 26.97$ d), the (n,γ) reaction cross sections were calculated using the ^{233}Pa characteristic γ line of 311.9 keV measured from 5–7 days cooled spectra. The number of counts measured from the respective decay spectra of ^{233}Th, with all other spectroscopic details taken from Ref. [37], were used in the equation

$$\langle\sigma_R\rangle = \frac{C_{\rm obs}\lambda\left(\frac{\rm CL}{\rm LT}\right)}{N_0\langle\Phi\rangle I_\gamma\epsilon(1-e^{-\lambda t_i})(e^{-\lambda t_c})(1-e^{-\lambda LT})}. \quad (3)$$

Here, σ_R is the reaction cross section and the other symbols have their same meanings as in Eq. (2). Neutron flux (Φ) calculated from Eq. (2) is used in (3) for the calculation of σ_r. The experimentally measured cross sections for incident neutron energies of 10.95 ± 0.59, 13.97 ± 0.57, 14.98 ± 0.55, and 18.99 ± 0.65 MeV are 14.45 ± 3.48, 2.79 ± 0.71, 3.37 ± 0.69, and 1.16 ± 0.14 mb, respectively. Besides the n_0 group of neutrons, the n_1 group and tailing part also took part in the formation of ^{233}Th and thus in the population of ^{233}Pa. Therefore, to calculate the true value of the cross sections, the contributions from the tailing part of the neutron spectrum must be subtracted from the measured values. The contributions of the cross sections due to the tail region of the neutron spectrum for the ^{232}Th(n,γ) reaction have been estimated using the ENDF/B-VII.1 [38] and JENDL-4.0 [43] data by folding the cross sections with neutron flux distributions. The contribution for the tail region at the neutron energies of 10.95 ± 0.59, 13.97 ± 0.57, 14.98 ± 0.55, and 18.99 ± 0.65 MeV evaluated form ENDF/B-VII.1 [38] are 12.56, 1.458, 1.983, and 0.579 mb and from JENDL-4.0 [43] they are 12.76, 1.706, 2.315, and 0.682 mb respectively. Thus the true value of cross-sections after the tailing correction are 1.787, 1.207, 1.22, and 0.529 mb, respectively. The measured and the final cross-section values after the tailing corrections are given in Table II. The uncertainties associated with the measured cross sections come from the combination of two experimental data sets. This overall uncertainty is the quadratic sum of both statistical and systematic errors. The random error in the observed activity is primarily due to counting statistics, and is found to be 12–25%. The systematic errors are due to uncertainties in neutron flux estimation (≈7%), the irradiation time (≈2%), the detection efficiency calibration (≈3%), the half-life of the product nuclei, and the γ-ray abundances (≈2%). The overall uncertainty in the measurements up to this point is in the range of 12–25%, coming from the combination of statistical and systematic errors. Since we have used the ^{232}Th(n,f) reaction to measure the flux and all four targets were counted using the same detector geometry, there exists a correlation between the efficiency and the cross sections measured at the four neutron energies. Therefore, to minimize the errors propagating through various quantities into the measured cross sections, we have performed covariance analysis for the present measurement, which is given in the next section. The errors in the resulting cross sections after the tailing corrections were calculated using covariance analysis.

IV. COVARIANCE ANALYSIS

A. Uncertainty in detector efficiency

The efficiency of the HPGe detector is determined by using a standard ^{152}Eu source. The variation of the efficiency with γ-ray energy for detectors is geometry independent, while their absolute values depend on geometry. The geometry dependent

TABLE III. Partial uncertainties in the efficiency.

Energy (KeV)	Partial uncertainty ($\times 10^3$) due to attributes				Total uncertainty ($\times 10^3$) ($\sigma_{\varepsilon_{ii}}$)
	$r = 1(C)$	$r = 2(I_\gamma)$	$r = 3(N_0)$	$r = 4(T_{1/2})$	
121.8	0.500127	2.876885	5.807249	0.017511	6.500081
244	0.722310	1.573122	3.361365	0.010135	3.780916
344	0.258827	1.679963	2.528450	0.007624	3.046701
411	0.981793	0.887414	1.728683	0.005212	2.177107
778.9	0.332362	0.603551	1.104305	0.003329	1.301629
867	0.920560	0.634021	1.012019	0.003051	1.507849
964	0.242351	0.380814	0.893612	0.002694	1.001150
112	0.225001	0.403821	0.781149	0.002355	0.907687
1212	0.959746	0.394639	0.663224	0.001999	1.231553
1299	0.748385	0.324648	0.650048	0.001961	1.043093
1408	0.131442	0.241646	0.634347	0.001912	0.691426

TABLE IV. Covariance matrix ($V_\varepsilon \times 100$) for the detector efficiency.

0.004225										
0.001952	0.00143									
0.001468	0.00085	0.000928								
0.001004	0.000581	0.000437	0.000474							
0.000641	0.000371	0.000279	0.000191	0.000169						
0.000588	0.00034	0.000256	0.000175	0.000112	0.000227					
0.000519	0.0003	0.000226	0.000154	0.000099	0.00009	0.0001				
0.000454	0.00026	0.000196	0.000135	0.000086	0.000079	0.00007	0.000082			
0.000385	0.000223	0.000168	0.000115	0.000073	0.000067	0.000059	0.000052	0.000152		
0.000378	0.000219	0.000164	0.000112	0.000072	0.000066	0.000058	0.000051	0.000043	0.00012	
0.000368	0.000213	0.000160	0.00011	0.00007	0.000064	0.000057	0.00005	0.000042	0. 000041	0.000048

efficiency of the detector is given by the relation

$$\varepsilon = K_c \frac{C}{N_0 I_\gamma e^{-\lambda T} \Delta t}, \tag{4}$$

where N_0 is the disintegration rate of ^{152}Eu γ ray source at the time of manufacturing, λ is the decay constant, T is the time interval between the date of manufacturing and observation, I_γ is the absolute intensity of the particular γ ray, and K_c is the correction factor for the coincidence-summing effect [44]. The coincidence summing correction was performed using the EFFTRAN code [45].

The different sources of uncertainty in the calibration process, which propagate as the uncertainty in the efficiency of the detector, are from C, N_0, I_γ, and $T_{1/2}$. Therefore, the efficiency of the detector can be written as the function of four attributes as

$$\varepsilon = f(C, N_0, I_\gamma, T_{1/2}). \tag{5}$$

The uncertainties in the detector efficiency due to the four attributes can be calculated using the quadratic sum formula for 11 gamma lines as

$$\left(\frac{\Delta\varepsilon_i}{\varepsilon_i}\right)^2 = \left(\frac{\Delta C_i}{C_i}\right)^2 + \left(\frac{\Delta N_o}{N_0}\right)^2 + \left(\frac{\Delta I_{\gamma_i}}{I_{\gamma_i}}\right)^2 + (t\Delta\lambda)^2, \tag{6}$$

where the uncertainty in decay constant is

$$\Delta\lambda = \frac{0.693 T_{1/2}}{T_{1/2}^2}. \tag{7}$$

Further, the covariance matrix for these 11 measurements is given by

$$(V_\varepsilon)_{ij} = \sum_r e_{ir} S_{ijr} e_{jr} \tag{8}$$

where S_{ijr} is the microcorrelation between e_{ir} and e_{jr} due to the rth attribute [46]. The microcorrelations between different attributes have been assigned based on the assumptions given in Refs. [41,47].

TABLE V. Measured efficiencies with correlation matrix.

E_γ (KeV)	Efficiency	Correlation matrix	
311.90	0.229286 ± 0.002785	1	
743.36	0.098438 ± 0.001195	0.904	1

The partial uncertainties related to four attributes are given in Table III and the covariance matrix (of dimension 11) related to detector efficiency is given in Table IV. Since the γ rays taken into calculations are different from those taken into account for efficiency calculations, the detector efficiencies for ^{97}Zr ($E_\gamma = 743.36$ KeV) and ^{233}Pa ($E_\gamma = 311.90$ KeV) was calculated using the model interpolation [41]

$$\ln \varepsilon_i = \sum_m p_m (\ln E_i)^{m-1}, \tag{9}$$

where p_m is the fitting parameter, m is the order of the model used for fitting, and E_i is the energy of the γ lines. The solution for Eq. (9) can be obtained by considering a linear model $Z = AP$, where, Z is a column matrix with its elements are defined as $z_i = \ln \varepsilon_i$, A is the design matrix with elements, $A_{im} = (\ln E_i)^{m-1}$, and P is the matrix having elements p_m. Parameters p_m can be estimated using the least-squares method. The covariance matrix for solution parameters is given by $V_{\hat{P}} = (A' V_z^{-1} A)^{-1}$. Now the values of parameters p_m can be calculated as

$$\hat{P} = V_{\hat{P}} \left(A' V_z^{-1} Z\right), \tag{10}$$

where matrix V_z can be obtained using $(V_z)_{ij} = \frac{(V_\epsilon)_{ij}}{\langle\epsilon_i\rangle\langle\epsilon_j\rangle}$. The goodness of the fit can be calculated by $\chi_m^2 = (Z - AP)' V_z^{-1} (Z - AP)$ [41]. Using Eq. (10) we obtain $\hat{P} = (-2.568, -0.860, -0.1383, -0.3045, -0.1088)$ with $\chi_m^2 = 1.33$. The calculated efficiencies and the corresponding correlation matrix for characteristic γ lines 311.90 and 743.36 KeV using $\hat{P}$ and $V_{\hat{P}}$ are given in Table V.

B. Uncertainty in the cross-section measurement

Following the ratio measure technique [48] for covariance analysis in activation cross-section measurement, by using Eq. (2) in Eq. (3), we can redefine Eq. (3) for the present measurement (r) and the monitor reaction (m) as

$$\langle\sigma_r\rangle = \langle\sigma_m\rangle Y_f \frac{C_r \varepsilon_m I_{\gamma_m} f_{\lambda_m}}{C_m \varepsilon_r I_{\gamma_r} f_{\lambda_r}}, \tag{11}$$

with the time factor f defined as

$$f = (1 - e^{-\lambda t_i})(e^{-\lambda t_c})(1 - e^{-\lambda LT})/\lambda. \tag{12}$$

TABLE VI. Monitor [^{232}Th(n, f)] cross sections [38] and ^{97}Zr fission yield [40].

E_n (MeV)	Cross section (mb)	Fission yield (%)
10.95	213.06 ± 3.40	3.40 ± 0.14
13.97	276.12 ± 4.43	
14.98	298.22 ± 5.07	
18.99	392.28 ± 6.66	

According the quadratic sum formula, the uncertainties are related to the parameters in Eq. (11) as

$$\left(\frac{\Delta\sigma_r}{\sigma_r}\right)^2 = \sum_a \left(\frac{\Delta a_r}{a_r}\right)^2 + \sum_a \left(\frac{\Delta a_m}{a_m}\right)^2 + \left(\frac{\Delta\sigma_m}{\sigma_m}\right)^2 + \left(\frac{\Delta Y_f}{Y_f}\right)^2,$$
$$a = a(C, \varepsilon, I_\gamma, f). \tag{13}$$

Since the decay constant is related to the cross section through the exponential function, the uncertainty in the time factor should be propagated from the uncertainty in the decay constants by

$$\left(\frac{\Delta f}{f}\right)^2 = s_{f\lambda}^2 \left(\frac{\Delta\lambda}{\lambda}\right)^2, \tag{14}$$

with the relative sensitivity given by

$$s_{f\lambda} = \left(\frac{\lambda t_i e^{-\lambda t_i}}{1 - e^{-\lambda t_i}} - \lambda t_c + \frac{\lambda(LT) e^{-\lambda(LT)}}{1 - e^{-\lambda(LT)}} - 1\right). \tag{15}$$

In order to reduce the partial uncertainty in measured efficiencies, we have calculated $\eta_{m,r} = \epsilon_m/\epsilon_r$. The fractional uncertainty $\Delta\eta_{m,r}/\eta_{m,r}$ is thus given by $\mathrm{var}(\eta_{m,r}) = \mathrm{var}(\epsilon_m) + \mathrm{var}(\epsilon_r) - 2\,\mathrm{cov}(\epsilon_m, \epsilon_r)$ and is found to be 0.414%. The fission yield and the respective uncertainty (4.117%) for ^{97}Zr were taken from the data by England and Rider [40] and are given in Tables VI and VII, respectively. The England and Rider data [40] contains evaluated fission yields, and the respective uncertainty could be up to $\approx 50\%$. A similar study has also been performed by Sivashankar *et al.* [41] by taking the ^{97}Zr fission yield for 14 MeV neutrons. Furthermore, one experimental datum measured by Sadhana Mukerji *et al.* [42] using the similar ^{7}Li(p, n) reaction as neutron generator, at the BARC-TIFR Pelletron in Mumbai, gives the uncertainty in the fission yield for ^{97}Zr as $3.14 \pm 0.15\%$, which is similar to the fission yield data by England and Rider [40]. Since, the experimental fission yield data are very limited, we are assuming the 14 MeV fission yield value to be constant in the neutron energy range 11–19 MeV. The present data can also be normalized with the available experimentally measured fission yields in future. The values given in Tables I and VI were used to calculate the partial error in each attribute. The partial uncertainties and correlation coefficients from each attribute in Eq. (11) are summarized in Table VII.

TABLE VIII. Covariance matrix (%) and corresponding correlation coefficients for the measured ^{232}Th(n, γ) cross sections.

E_n (MeV)	Covariance matrix ($V_{cs_{ij}}$)				Correlation matrix			
10.95	4.5342				1			
13.97	0.1821	1.20234			0.078	1		
14.98	0.1821	0.1821	4.3657		0.041	0.079	1	
18.99	0.1821	0.1821	0.1821	2.6055	0.053	0.102	0.054	1

Using the definition given in Eq. (8), the final covariance matrix ($V_{cs_{ij}}$) is generated by adding all the matrices from each attribute with the correlation matrix, as given in Table VIII. The uncertainty in the measured cross sections now can be calculated by taking the square root of diagonal elements $[(V_{cs_{ii}})^{1/2}]$ of the covariance matrix. The tailing corrected cross sections with the calculated uncertainties from the covariance analysis along with the cross-section values calculated using ENDF-B/VII.1 and JENDL-4.0 data libraries and TALYS-1.8 are given in Table IX.

V. RESULT AND DISCUSSIONS

The cross sections for the ^{232}Th(n, γ) reaction at the average neutron energies of 10.95 ± 0.59, 13.97 ± 0.57, 14.98 ± 0.55, and 18.99 ± 0.65 MeV have been measured. The uncertainties in the present work have been analyzed using the covariance technique and the ratio measurement method, which is a well-established procedure for the uncertainty analysis in neutron-induced reactions. In the present experiment, the cross sections at each neutron energy, have been measured relative to the monitor cross section ^{232}Th(n, f). All the attributes, except for efficiency, involved in the cross-section calculation of ^{232}Th(n, γ) have been measured individually in the present experiment. However, due to the use of the same detector geometry and the monitor reaction for each measurement, there exists a correlation between the errors of all the parameters, which leads to the final covariance matrix, given in Table VIII. The errors propagated through all the parameters into the

TABLE VII. Fractional uncertainties in various parameters to obtain ^{232}Th(n, γ) cross section.

E_n (MeV)	Partial uncertainty (%)								
	C_r	C_m	I_{γ_r}	I_{γ_m}	$\eta_{r,x}$	f_{λ_r}	f_{λ_m}	Y_f	σ_W
10.95	10.755	17.803	1.038	0.0174	0.414	0.0421	0.0443	4.117	1.599
13.97	6.135	7.862	1.038	0.0174	0.414	0.0421	0.0443	4.117	1.603
14.98	6.623	19.277	1.038	0.0174	0.414	0.0421	0.0443	4.117	1.701
18.99	8.496	12.933	1.038	0.0174	0.414	0.0421	0.0443	4.117	1.698
Corr.	0	0	1	1	1	1	1	1	0

TABLE IX. ^{232}Th(n,γ) reaction cross sections at different neutron energies.

Neutron energy	Flux	Cross section (mb)			
(MeV)	n cm^{-2} s^{-1}	Measured	ENDF-B/VII.1	JENDL-4.0	TALYS-1.8
10.95 ± 0.59	5.65×10^6	1.787 ± 0.378	1.180	1.495	1.174
13.97 ± 0.57	2.35×10^6	1.207 ± 0.132	1.153	1.159	1.155
14.98 ± 0.55	1.64×10^6	1.22 ± 0.25	0.843	0.923	0.821
18.99 ± 0.65	8.49×10^6	0.529 ± 0.085	0.214	0.499	0.225

cross-section measurement have also been determined and are tabulated in Table VIII. The experimentally measured cross-section data for the ^{232}Th(n,γ) reaction at the above neutron energies were also compared with the values from the literature [24,28–30,33] and from ENDF/B-VIII.1 [38] and JENDL-4.0 [43] data libraries, and are given in Table IX. Figure 3 shows the present experimental data along with the literature data [22–24,28–33,49]. The theoretical values from nuclear data libraries are also used to examine the trend of cross section within the range of neutron energies of the present work. It can be observed from Fig. 3 that most of the experimental data from different authors [22–24,31–33,49] were concentrated below 6 MeV and the observed trend of cross section decreases monotonically. Beyond 6 to 7 MeV, the reaction cross section for ^{232}Th(n,γ) again increases. The dip in the ^{232}Th(n,γ) reaction cross section around a neutron energy of 6–7 MeV is due to the opening of ^{232}Th$(n,2n)$ reaction channel, having a threshold energy of 6.44 MeV. In order to examine this, the ^{232}Th$(n,2n)$ reaction cross section from the literature [24,27–30,50–53] as well as from the evaluated ENDF/B-VIII.1 [36] and JENDL-4.0 [43] data libraries are plotted in Fig. 4. It can be seen from Fig. 4 that the ^{232}Th$(n,2n)$ reaction cross section increases sharply from its threshold value of 6.44 to 8 MeV. Thereafter it remains constant up to the neutron energy of 14 MeV. Thus, beyond the neutron energy of 8 MeV, the ^{232}Th(n,γ) reaction cross sections increase up to 10 MeV and then remain nearly constant up to 14 MeV due to the nearly constant value of the ^{232}Th$(n,2n)$ reaction cross section. Beyond the neutron energy of 14 MeV, the ^{232}Th$(n,3n)$ reaction channels open up and thus both the ^{232}Th(n,γ) and ^{232}Th$(n,2n)$ reaction cross sections decrease. These observations indicate the partition of energy in different reaction channels. Since very limited work has been carried out in this region [28–30,33], the reaction cross-section data were measured in the present work and are found to be in good agreement with the literature data [28–30] and the evaluated data of ENDF/B-VIII.1 and JENDL-4.0 data libraries. However, the data of Perkin *et al.* [33] around a neutron energy of 14 MeV based on the $D+T$ neutron source are unusually high. This is most probably due to the contribution of cross sections from low energy scattered neutrons from the $D+T$ neutron source. We have also tried to fit the present experimental as well as the literature data using theoretical nuclear modular code TALYS-1.8 [54] using default as well as adjusted parameters.

TALYS is a computer code that can be used to calculate the reaction cross-section based on physics models and parametrizations. In the present work, we have calculated the ^{232}Th(n,γ) reaction cross section by using default and adjusted parameters. All possible outgoing channels in the neutron-induced reactions of ^{232}Th were considered. The level density parameters were adjusted accordingly to get a better agreement with the experimental values and literature data. In the present calculation, the energy dependence of

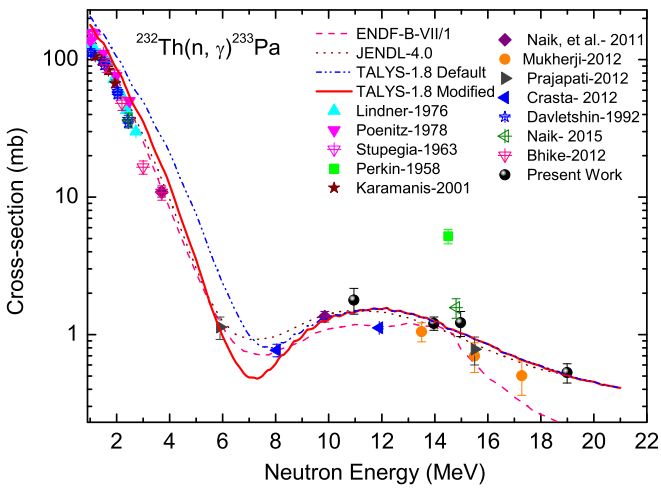

FIG. 3. Comparison of the present experimental ^{232}Th$(n,\gamma)^{233}$Th reaction cross sections with the literature data [22–26,28–33,49], evaluated data [38,43], and theoretical values [54].

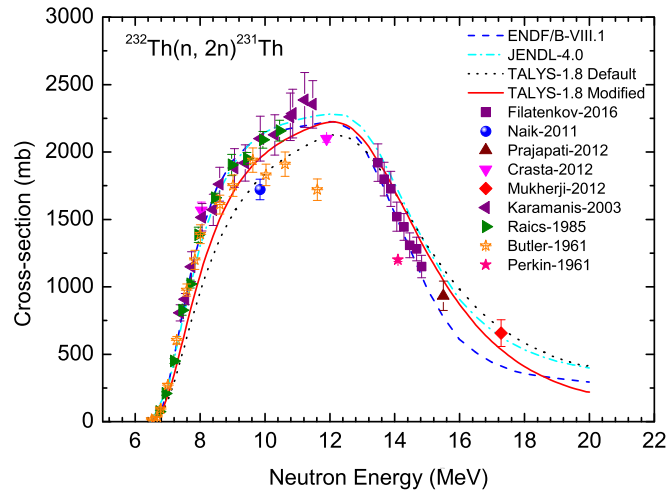

FIG. 4. Comparison of ^{232}Th$(n,2n)^{231}$Th reaction cross sections with the literature data [24,27–30,50–53], evaluated data [38,43], and theoretical values [54].

TABLE X. Default and adjusted parameters used in the TALYS-1.8 calculations.

Parameter	CTM collective		CTM effective	
	Default value	Adjusted value for ^{232}Th(n,γ)	Default value	Adjusted value for ^{232}Th$(n,2n)$
α	0.02073	0.02073	0.06926	0.01556
β	0.22953	0.22953	0.28277	0.28277
γ_1	0.47362	0.79462	0.4309	0.4309

the level-density parameter plays a very important role. The level-density parameter (a) varies with energy according to the equation

$$a = \tilde{a}\left[1 + \delta\epsilon_0\left(\frac{1 - e^{-\gamma U}}{U}\right)\right], \tag{16}$$

with U defined as

$$U = E_x - \Delta, \tag{17}$$

where $\tilde{a}$ is the asymptotic value of a at high excitation energy (E_x), and $\delta\epsilon_0$ is the shell correction of the nuclear binding energy, whose magnitude establishes how a is different from $\tilde{a}$ at low energies. The sign of the shell correction term $\delta\epsilon_0$ regulates whether $a(U)$ increases or decreases as a function of effective excitation energy U. Δ is the energy shift which is included to simulate the odd-even effects in nuclei, and γ is the damping parameter, which governs how fast λ approaches $\tilde{a}$ and can be given as $\gamma = \frac{\gamma_1}{A^{1/3}} + \gamma_2$. The level-density parameter shows the presence of shell effects at low energy and their disappearance at high energy in a phenomenological manner. The asymptotic value of $\tilde{a}$ is given by

$$\tilde{a} = \alpha A + \beta A^{2/3}, \tag{18}$$

where A is the mass number, and α, β, and $\gamma_{1,2}$ are global parameters that have been determined to give the best average level density description over a whole range of nuclides [54]. Table X shows the values of default and adjusted parameters of TALYS-1.8 calculation used in the present work. As default, TALYS uses the constant temperature model (CTM, effective + collective) [55] with "ldmodel1" parameters. For the present case, we have used CTM (collective) with a different set of parameters as given in Table X. The ^{232}Th(n,γ) reaction cross-section values obtained from TALYS-1.8 based on adjusted parameters are plotted in Fig. 3 and are found to be in good agreement with the experimental data of the present work and literature. It can also be seen from Fig. 3 that TALYS-1.8 (default) also satisfactorily reproduces that cross sections over the entire range (1–25 MeV) of study. Although the cross sections obtained from TALYS-1.8 (default) are slightly higher than measured and evaluated data, the trend is reproduced quite well. Figure 3 also shows that ENDF/B-VIII.1 evaluated data start decreasing around 15 MeV and are not in agreement with JENDL-4.0 as well as with TALYS-1.8 data. Moreover, experimental data also seems to be in generally good agreement with the latter.

The ^{232}Th$(n,2n)$ reaction cross-section values obtained from TALYS-1.8 with the default and adjusted parameters are plotted in Fig. 4. In this case, we have used CTM-effective while changing single-particle level density parameter g. The single-particle level density parameter g can be written as $g = A/K_{\rm ph}$, where A is the atomic mass and $K_{\rm ph}$ is a constant. The fitting was done using adjusted parameters for CTM-effective (Table X), keeping $K_{\rm ph} = 10$. It can be seen from Fig. 4 that the ^{232}Th$(n,2n)$ reaction cross-section values from TALYS-1.8 with the adjusted parameters fit very well with the previous experimental data [24,27–30,50–53].

TALYS uses several models for the calculation of the γ-ray strength function. A standard Lorentzian form describes the giant dipole resonance shape in the Brink-Axel option [56], in which the energy dependent γ-ray strength function $f_{X\ell}(E_\gamma)$ for multipolarity ℓ of type X (type E or M) is given by

$$f_{X\ell}(E_\gamma) = K_{X\ell}\frac{\sigma_{X\ell}E_\gamma\Gamma_{X\ell}^2}{\left(E_\gamma^2 - E_{X\ell}^2\right)^2 + E_\gamma^2\Gamma_{X\ell}^2}, \tag{19}$$

where $\sigma_{X\ell}$, $E_{X\ell}$, and $\Gamma_{X\ell}$ are the strength, energy, and the width of the giant dipole resonance, respectively and $K_{Xl} = 1/(2\ell+1)\pi^2\hbar^2c^2$. TALYS uses the Brink-Axel option for all transition types other than $E1$. For $E1$ radiation, the default option used in TALYS is the generalized Lorentzian form of Kopecky and Uhl [57]. The γ-ray strength function for $E1$ under Kopecky and Uhl is given by

$$f_{E1}(E_{\gamma,T}) = K_{E1}\sigma_{E1}\Gamma_{E1}\left[\frac{E_\gamma\tilde{\Gamma}_{E1}}{\left(E_\gamma^2 - E_1^2\right)^2 + E_\gamma^2\Gamma_{E1}^2} + \frac{0.7\Gamma_{E1}4\pi^2T^2}{E_{E1}^3}\right], \tag{20}$$

the energy dependent damping fator $\tilde{\Gamma}_{E1}$ is given by

$$\tilde{\Gamma}_{E1} = \Gamma_{E1}\frac{E_\gamma^2 + 4\pi^2T^2}{E_{E1}^2}, \tag{21}$$

and the nuclear temperature T [58] is given by

$$T = \sqrt{\frac{E_n + S_n - \Delta - E_\gamma}{a(S_n)}}, \tag{22}$$

where S_n is the neutron separation energy, E_n the incident neutron energy, Δ the pairing correction, and a is the level density parameter at S_n. The computed γ strength parameters for both the TALYS fits have been calculated and are presented in Table XI. For $E1$ transitions systematic formulas compiled by Kopecky [59] were used, whereas for $E2$ transitions the Brink-Axel options were used as default by TALYS.

TABLE XI. γ-ray strength function parameters for giant dipole resonance.

Multipole transition	γ-ray strength function parameters			
	$\sigma_0(X\ell)$	$E(X\ell)$	$\Gamma(X\ell)$	$K(X\ell)$
$M1$	1.078	6.663	4.000	8.67×10^{-8}
$E1$	687.477	13.375	3.314	8.67×10^{-8}
$M2$	0.001	6.663	4.000	5.20×10^{-8}
$E2$	0.569	10.238	3.314	5.20×10^{-8}

VI. CONCLUSIONS

The ^{232}Th(n,γ) reaction cross sections were measured at neutron energies of 10.95 ± 0.59, 13.97 ± 0.57, 14.98 ± 0.55, and 18.99 ± 0.65 MeV. The uncertainty in the present measurements has been calculated with covariance analysis and is found in the range 10–20%. The results from the present work are compared with existing literature data along with the values of ENDF/B-VIII.1 and JENDL-4.0 data libraries and are found to be in good agreement. The ^{232}Th (n,γ) reaction cross sections were also calculated theoretically by using the TALYS-1.8 code with default as well as adjusted parameters. TALYS (default) does not reproduce the experimental data of the present work and literature as well as the data of different libraries for the neutron energies within 1 and 7 MeV. However, for $E_n > 7$ MeV, TALYS satisfactorily reproduces the experimental data and is in good agreement with JENDL-4.0. On the other hand, TALYS with an adjusted set of parameters satisfactorily reproduces the (n,γ) and $(n,2n)$ reaction cross sections of ^{232}Th in the entire energy range. The different decreasing and increasing trends of the (n,γ) and $(n,2n)$ reaction cross sections of ^{232}Th with neutron energy show the partition of energy in different reaction channels.

ACKNOWLEDGMENTS

One of the authors (S.M.) thanks the Department of Atomic Energy-Board of Research in Nuclear Sciences (DAE-BRNS) for the financial support in the form of a major research project (Sanction Number 36(6)/14/22/2016-BRNS). The authors are thankful to the staff of Pelletron facility at Tata Institute of Fundamental Research (TIFR), Mumbai for their excellent operation of the accelerator.

[1] S. K. Malhotra, Extending the global reach of nuclear energy through thorium, Public Awareness Division, Department of Atomic Energy, Govt. of India, September 2008, http://dae.nic.in/writereaddata/.pdf_38

[2] C. Rubbia, J. A. Rubio, S. Buono, F. Carminati, N. Fietier, J. Galvez, C. Geles, Y. Kadi, R. Klapisch, P. Mandrilion, J. P. Revol, and Ch. Roche, Conceptual design of a fast neutron operated high power energy amplifier, CERN Report No. CERN/AT/95-44 (ET), 1995, http://cds.cern.ch/record/289551/files/cer-0210391.pdf.

[3] C. D. Bowman *et al.*, Nuclear energy generation and waste transmutation using and accelerator-driven intense thermal neutron source, International conference on emerging nuclear energy systems, Monterey, CA (United States), 1991 [Los Alamos National Laboratory Report No. LA-UR-91-2601].

[4] C. D. Bowman, Annu. Rev. Nucl. Part. Sci. **48**, 505 (1998).

[5] F. Carminati, R. Klapisch, J. P. Revol, Ch. Roche, J. A. Rubio, and C. Rubbia, An energy amplifier for cleaner and inexhaustible nuclear energy production driven by particle beam accelerator, CERN Report No. CERN/AT/93-47 (ET), 1993, http://cds.cern.ch/record/256520/files/at-93-047.

[6] *The International Conference on Accelerator-Driven Transmutation Technologies and Applications*, Las Vegas, 1994, edited by E. D. Arthur, S. A. Schriber, and A. Rodriguez, AIP Conf. Proc. No. 346 (AIP, New York, 1995).

[7] Accelerator driven systems: Energy generation and transmutation of nuclear waste, status report, IAEA Report No. TECDOC-985, 1997 (unpublished).

[8] S. Ganesan, Pramana J. Phys. **68**, 257 (2007).

[9] R. K. Sinha and A. Kakodkar, Nucl. Eng. Des. **236**, 683 (2006).

[10] S. Ganesan, Creation of Indian experimental benchmarks for thorium fuel cycle, in IAEA Coordinated Research Project on Evaluated Data for Thorium-Uranium fuel Cycle, Third Research Co-ordination Meeting, 30 January to 2 February 2006, Vienna, Austria, IAEA Report No. INDC (NDS)-0494, 2006 (unpublished).

[11] Thorium fuel utilization: Options and trends, Fast Reactors and Accelerator Driven Systems Knowledge Base, IAEA Report No. TECDOC-1319, 2002 (unpublished).

[12] A. Nuttin, D. Heuer, A. Billebaud, R. Brissot, C. Le Brun, E. Liatard, J.-M. Loiseaux, L. Mathieu, O. Meplan, E. Merle-Lucotte, H. Nifenecker, F. Perdu, and S. David, Proc. Nucl. Energy **46**, 77 (2005).

[13] T. R. Allen and D. C. Crawford, Sci. Technol. Nucl. Install. **2007**, 97486 (2007).

[14] V. G. Pronyaev, Summary report of the consultants' meeting on assessment of nuclear data needs for thorium and other advanced cycles, INDC (NDS)-408 (1999).

[15] B. D. Kuz'minov and V. N. Manokhin, Nucl. Constants (International Nuclear Data Committee), Issue Number 3–4, p. 41 (1997), http://www.iaea.org/inis/collection/NCLCollectionStore/_Public/29/062/29062825.pdf.

[16] D. E. Bartine, The use of thorium in fast breeder reactors, in Proceedings of the International Conference on Nuclear Cross Sections for Technology, Knoxville, Tennessee, October 22–26, 1979 [Natl. Bur. Stand. Spec. Pub. **594**, 119 (1980)].

[17] Pelloni, G. Youinou, and P. Wydler, Impact of different nuclear data on the performance of fast spectrum based on the thorium-uranium fuel cycle, in *Proceedings of the International Conference on Nuclear Data for Science and Technology*, Trieste, Italy, May 19–24, 1997 (Italian Physical Society, Bologna, 1997), Vol. 59, Part II, p. 1172.

[18] M. Salvatores, in *Proceedings of the International Conference on Nuclear Data for Science and Technology*, Trieste, Italy, May 19–24, 1997, edited by G. Reffo, A. Ventura, and C. Grandi (Italian Physical Society, Bologna, 1997), Vol. 59, Part I, pp. 3–17.

[19] R. C. Little, R. C. Block, D. R. Harris, R. E. Slovacek, and O. N. Carlson, Nucl. Sci. Eng. **79**, 175 (1981).

[20] Borella, K. Volev, A. Brusegan, P. Schillebeeckx, F. Corvi, N. Koyumdjieva, N. Janeva, and A. A. Lukyanov, Nucl. Sci. Eng. **152**, 1 (2006).

[21] G. Aertset *et al.*, Phys. Rev. C **73**, 054610 (2006).

[22] D. C. Stupegia, B. Smith, and K. Hamm, J. Inorg. Nucl. Chem. **25**, 627 (1963).

[23] M. Lindner, R. J. Nagle, and J. H. Landrum, Nucl. Sci. Eng. **59**, 381 (1976).

[24] H. Naik, P. M. Prajapati, S. V. Surayanarayana, K. C. Jagadeesan, S. V. Thakare, D. Raj, V. K. Mulik, B. S. Sivashankar, B. K. Nayak, S. C. Sharma, S. Mukherjee, S. Singh, A. Goswami, S. Ganesan, and V. K. Manchanda, Eur. Phys. J. A **47**, 51 (2011).

[25] H. Naik, S. V. Surayanarayana, S. Bishnoi *et al.*, J. Radioanal. Nucl. Chem. **303**, 2497 (2015).

[26] M. Bhike, B. J. Roy, A. Saxena, R. K. Choudhury, and S. Ganesan, J. Nucl. Sci. Eng. **170**, 44 (2012).

[27] D. Karamanis, S. Andriamonje, P. A. Assimakopoulos, G. Doukellis, D. A. Karadimos, A. Karydas, M. Kokkoris, S. Kossionides, N. G. Nicolis, C. Papachristodoulou, C. T. Papadopoulos, N. Patronis, P. Pavlopoulos, G. Perdikakis, and R. Vlastou (The n-TOF Collaboration), Nucl. Instrum. Methods Phys. Res. A **505**, 381 (2003).

[28] S. Mukherji, H. Naik, S. V. Suryanarayanan, S. Chachara, B. S. Shivashankar, V. Mulik, R. Crasta, S. Samanta, B. K. Nayak, A. Saxena, S. C. Sharma, P. V. Bhagwat, K. K. Rasheed, R. N. Jindal, S. Ganeshan, A. K. Mohantey, A. Goswami, and P. D. Krishnani, Pramana **79**, 249 (2012).

[29] P. M. Prajapati, H. Naik, S. V. Suryanarayana, S. Mukherjee, K. C. Jagadeesan, S. C. Sharma, S. V. Thakre, K. K. Rasheed, S. Ganesan, and A. Goswami, Eur. Phys. J. A **48**, 35 (2012).

[30] R. Crasta, H. Naik, S. V. Suryanarayana, B. S. Shivashankar, V. K. Mulik, P. M. Prajapati, G. Sanjeev, S. C. Sharma, P. V. Bhagwat, A. K. Mohanty, S. Ganesan, and A. Goswami, Ann. Nucl. Energy **47**, 160 (2012).

[31] W. P. Poenitz and D. L. Smith, Fast neutron radiative capture cross sections of ^{232}Th, Argonne National Laboratory Report No. ANL-NDM-42, 197803, 1978 (unpublished).

[32] A. N. Davletshin, E. V. Teplov, A. O. Tipunkov, V. A. Tolstikov, I. A. Korzh, V. D. Ovdienko, N. M. Pravdivyy, N. T. Sklyar, and V. A. Mishchenko, J. Yad. Konst. **41**, 1992 (1992).

[33] J. L. Perkin, L. P. O'Connor, and R. F. Colemann, Proc. Phys. Soc. London **72**, 505 (1958).

[34] J. F. Ziegler, Nucl. Instrum. Methods B **219–220**, 1027 (2004).

[35] C. H. Poppe, J. D. Anderson, J. C. Davis, S. M. Grimes, and C. Wong, Phys. Rev. C **14**, 438 (1976).

[36] S. G. Mashnik, M. B. Chadwick, H. G. Hughes, R. C. Little, R. E. Macfarlane, L. S. Waters, and P. G. Young ^{7}Li(p, n) Nuclear data library for incident proton energies to 150 MeV, Los Alamos National Laboratory, Report NM 87545, USA (2008), arXiv:nucl-th/0011066v1.

[37] NuDat 2.7β, 2011, National Nuclear Data Center, Brookhaven National Laboratory, http://www.nndc.bnl.gov/

[38] ENDF/B-VII.1, 2011, National Nuclear Data Center, Brookhaven National Laboratory, http://www.nndc.bnl.gov/exfor/endf00.jsp

[39] R. Makwana *et al.*, Phys. Rev C **96**, 024608 (2017).

[40] T. R. England and B. F. Rider, Evaluation and compilation of fission product yields, 1993, ENDF-349, Los Alamos Report No. LA-UR-94-3106, final document September 1994, https://t2.lanl.gov/nis/publications/endf349.pdf.

[41] B. S. Shivashankar, S. Ganesan, H. Naik, S. V. Suryanarayan, N. Sreekumaran Nair, and K. Manjunathan Prasad, Nucl. Sci. Eng. **179**, 423 (2015).

[42] S. Mukerji, H. Naik, and S. V. Suryanarayana, Proc. DAE Symp. Nucl. Phys. **59**, 426 (2014).

[43] K. Shibata, O. Iwamoto, T. Nakagawa, N. Iwamoto, A. Ichihara, S. Kunieda, S. Chiba, K. Furutaka, N. Otuka, T. Ohsawa, T. Murata, H. Matsunobu, A. Zukeran, S. Kamada, and J. Katakura, J. Nucl. Sci. Technol. **48**, 1 (2011).

[44] T. M. Semkow, G. Mehmood, P. P. Parekh, and M. Virgil, Nucl. Instrum. Methods Phys. Res. A **290**, 437 (1990).

[45] T. Vidmar, G. Kanish, and G. Vidmar, Appl. Radiat. Isot. **69**, 908 (2011).

[46] L. P. Geraldo and D. Smith, Nucl. Instrum. Methods Phys. Res. A **290**, 499 (1990).

[47] W. Mannhart, IAEA Report No. INDC(NDS)-0588 Rev., 2013, https://www-nds.iaea.org/publications/indc/indc-nds-0588/.

[48] N. Otuka *et al.*, Radiat. Phys. Chem. **140**, 502 (2017).

[49] D. Karamanis, M. Petit, S. Andriamonje, G. Barreau, M. Bercion, A. Billebaud, B. Blank, S. Czajkowski, R. Del Moral, J. Giovinazzo, V. Lacoste, C. Marchand, L. Perrot, M. Pravikoff, and J. C. Thomas, Nucl. Sci. Eng. **139**, 282 (2001).

[50] A. A. Filatenkov, Neutron activation cross sections measured at KRI in neutron energy region 13.4–14.9 MeV, I.N.D.C. USSR Report No. 0460, 2016 (unpublished).

[51] P. Raics, S. Daroczy, J. Csikai, N. V. Kornilov, V. Ya. Baryba, and O. A. Salnikov, Phys. Rev. C **32**, 87 (1985).

[52] J. L. Perkin and R. F. Coleman, Nucl. Energy A/B, Reactor Sci. Technol. **14**, 69 (1961).

[53] J. P. Butler and D. C. Santry, Can. J. Chem. **39**, 689 (1961).

[54] A. J. Koning, S. Hilaire, and S. Goriely, *TALYS User Manual: A Nuclear Reaction Program*, NRG-1755 (Nuclear Research and Consultancy Group, Petten, The Netherlands, 2015).

[55] A. Gilbert and A. G. W. Cameron, Can. J. Phys. **43**, 1446 (1965).

[56] D. M. Brink, Nucl. Phys. **4**, 215 (1957); P. Axel, Phys. Rev. **126**, 671 (1962).

[57] J. Kopecky and M. Uhl, Phys. Rev. C **41**, 1941 (1990).

[58] J. Kopecky, M. Uhl, and R. E. Chrien, Phys. Rev. C **47**, 312 (1993).

[59] R. Capote *et al.*, RIPL - Reference input parameter library for calculation of nuclear reactions and nuclear data evaluation, Nucl. Data Sheets **110**, 3107 (2009).